

## Electronic Supplementary Information for

# Temperature-Responsive Smart Molecule Gate in Metal-Organic Framework for Task-Specific Gas Separation

**Qiang Tan,<sup>a,b</sup> Hongliang Huang,<sup>\*a,c</sup> Yaguang Peng,<sup>b</sup> Yanjiao Chang,<sup>a,c</sup>  
Zhengqing Zhang,<sup>a,c</sup> Dahuan Liu<sup>\*b</sup> and Chongli Zhong<sup>\*a,b,c</sup>**

<sup>a</sup> State Key Laboratory of Separation Membranes and Membrane Processes, Tianjin Polytechnic University, Tianjin 300387, China

<sup>b</sup> State Key Laboratory of Organic-Inorganic Composites, Beijing University of Chemical Technology, Beijing 100029, China

<sup>c</sup> School of Chemistry and Chemical Engineering, Tianjin Polytechnic University, Tianjin 300387, China

## Materials.

All of the solvents and reagents were commercially available and used without further purification.

## Preparation of MOFs.

CAU-10-X were synthesized according to the reported method<sup>1</sup> with minor modifications.

CAU-10-OMe: A solution containing  $\text{Al}_2(\text{SO}_4)_3 \cdot 18\text{H}_2\text{O}$  (2.04 g, 3.06 mmol), 5-methoxysiophthalic acid (1.20 g, 3.06 mmol), N, N'-dimethylformamide (DMF, 3 ml) and  $\text{H}_2\text{O}$  (12 ml) was transferred to the Teflon-line stainless steel autoclave. This reaction was heated at  $130^\circ\text{C}$  for 12 h under autogenous pressure. After cooling down to room temperature, the product was filtered off. Subsequently, the obtained product was treated by sonication and stirring in water, until form a homogeneous mixture. The dispersion was filtered again and the obtained powder was washed with deionized water and fresh acetone for several times. After that, the obtained white crystals were heated at  $150^\circ\text{C}$  under vacuum overnight.

CAU-10-H:  $\text{Al}_2(\text{SO}_4)_3 \cdot 18\text{H}_2\text{O}$  (1.20 mmol, 800 mg) and isophthalic acid (1.20 mmol, 200 mg) were dissolved in DMF (1 ml) and  $\text{H}_2\text{O}$  (4 ml) in a Teflon-line stainless steel autoclave. The mixture was heated at  $135^\circ\text{C}$  for 12 h. Afterward, the product was cooled down to room temperature and collected by filtered. The obtained solid was stirred under sonication in water. Therefore, the mixture was filtered again and then washed with deionized water and acetone for several times. Finally, the white microcrystalline was dried at  $150^\circ\text{C}$  for 12 h under vacuum.

CAU-10-NH<sub>2</sub>: 2 M  $\text{AlCl}_3 \cdot 6\text{H}_2\text{O}$  water solution (6.6mmol  $\text{Al}^{3+}$ , 3.3ml) and 5-aminoisophthalic acid (6.63 mmol, 1200mg) were dissolved in DMF (4 ml) and  $\text{H}_2\text{O}$  (12.7 ml) in a glass reactor with screw cap. The mixture was heated at  $120^\circ\text{C}$  for 12 h. Afterward, the product was cooled down to room temperature and collected by filtered. The obtained solid was stirred under sonication in water. Therefore, the mixture was

filtered again and then washed with deionized water and acetone for several times. Finally, the white microcrystalline was dried at 150°C for 12 h under vacuum.

CAU-10-NO<sub>2</sub>: 2 M AlCl<sub>3</sub>·6H<sub>2</sub>O water solution (6.80 mmol Al<sup>3+</sup>, 3.4 ml) and 5-nitroisophthalic acid (6.82 mmol, 1440 mg) were dissolved in DMF (4 ml) and H<sub>2</sub>O(12.6 ml) in a glass reactor with screw up. The mixture was heated at 120°C for 12 h. Afterward, the product was cooled down to room temperature and collected by filtered and the product was processed in the same way as CAU-10-NH<sub>2</sub>.

CAU-10-F: 0.5 M Al<sub>2</sub>(SO<sub>4</sub>)<sub>3</sub>·18H<sub>2</sub>O solution (6.88 mmol Al<sup>3+</sup>, 6.88 ml) and 5-fluoroisophthalic acid (6.85 mmol, 1260 mg) were dissolved in DMF (4 ml) and H<sub>2</sub>O (9.12 ml) in a Teflon-line stainless steel autoclave. The mixture was heated at 120°C for 12 h. Afterward, the product was cooled down to room temperature and collected by filtered. The obtained solid was stirred under sonication in water. Therefore, the mixture was filtered again and then washed with deionized water and acetone for several times. Finally, the white microcrystalline was dried at 150°C for 12 h under vacuum.

### **Characterization**

The Fourier transform infrared (FT-IR) were measured on a Nicolet 6700 FTIR spectrophotometer. Power X-ray diffraction data (PXRD) were recorded on D8 Advanced X diffractometer with Cu K $\alpha$  radiation ( $\lambda$ = 1.5406 Å) at RT. The 2 $\theta$  was scanned ranging from 5° to 50° in 0.02° steps with a scan rate of 5°/min. Variable temperature powder X-ray diffraction (VT-PXRD) were recorded on a PANalytical X'PertPro. Fourier transform infrared (FTIR) measurements were recorded using a Thermo Nicolet iS50 FTIR (Thermo Fisher Scientific Co., MA, USA) spectrometer equipped with a single-bounce diamond crystal and a deuterated triglycine sulfate detector. Raman spectra were obtained using a Renishaw InVia Reflex spectrometer (Wotton-under-Edge, UK). The BET surface areas of the samples were done on a Micromeritics ASAP 2020 using N<sub>2</sub> adsorption data at 77 K.

## Gas Adsorption Measurement

Gas adsorption measurements were performed on a Micromeritics ASAP 2020 surface area and pore size analyzer. The sample tube filled with about 300 mg sample. Before the adsorption/desorption, the adsorbent was degassed under vacuum at 423 K for 12 h by using the “automatic degas” function of the analyzer. Ultrahigh purity grade N<sub>2</sub>, CH<sub>4</sub>, C<sub>2</sub>H<sub>4</sub>, C<sub>3</sub>H<sub>6</sub>, C<sub>3</sub>H<sub>8</sub> and i-C<sub>4</sub>H<sub>10</sub> were used for gas adsorption measurement. The temperatures at 87 K, 143 K, 175 K, 203 K, 213 K, 233 K, 273 K, 298 K, 323 K, 343 K were maintained with liquid argon bath, n-pentane-liquid nitrogen bath, methanol-liquid nitrogen bath, low temperature thermostat and thermostat, respectively.<sup>2,3</sup> To prevent condensation of CH<sub>4</sub> at 87 K, the pressure range was below 7.2 KPa. To prevent condensation of C<sub>2</sub>H<sub>4</sub> and C<sub>2</sub>H<sub>6</sub> at 143 K, the pressure range was below 15.8 KPa and 5.1 KPa. To prevent condensation of C<sub>3</sub>H<sub>6</sub> at 213 K, the pressure range was below 73.4 KPa. For all adsorption isotherms, we choose a relative saturation pressure given by the Micromeritics ASAP 2020 surface area and pore size analyzer during the measurements: at 87 K, N<sub>2</sub> was 100 KPa and CH<sub>4</sub> was 6.6 KPa; at 143 K, CH<sub>4</sub> was 100 KPa, C<sub>2</sub>H<sub>4</sub> was 14.5 KPa and C<sub>2</sub>H<sub>6</sub> was 5 KPa; at 213 K, C<sub>2</sub>H<sub>4</sub> was 100 KPa and C<sub>3</sub>H<sub>6</sub> was 71.7 KPa; at other temperature, all gases of measurement were 100 KPa. However, in order to facilitate the observation of molecular sieving effect, the minimum relative pressure of the measurement gases as the highest pressure on the abscissa of the graph was selected at a certain temperature.

## Ideal adsorption solution theory (IAST) calculations

The Dual-site Langmuir model was carried out by fitting adsorption isotherms of C<sub>3</sub>H<sub>6</sub> and C<sub>3</sub>H<sub>8</sub> in CAU-10-OMe at 298 K. The Dual-site Langmuir equation can be defined as,

$$q = q_A + q_B = q_{sat,A} \frac{b_A p}{1 + b_A p} + q_{sat,B} \frac{b_B p}{1 + b_B p}$$

Where,  $q$  is a molar loading of adsorbate;  $q_{sat}$  is a saturation loading;  $b$  is coefficient in the pure component Langmuir adsorption isotherm;  $A$  and  $B$  refer to two different

sites on the molecules. The adsorption selectivity for the C<sub>3</sub>H<sub>6</sub>:C<sub>3</sub>H<sub>8</sub> (50:50 v/v %) can be defined by

$$s = \frac{q_1 p_2}{q_2 p_1}$$

Where,  $q_i$  is the quantity adsorbed of component  $i$ ;  $p_i$  represents the partial pressure of the component  $i$ .

### Density functional theory calculations

All quantum chemistry calculations were performed by using the plane wave density functional theory (DFT) implemented in the Vienna ab initio simulation package (VASP).<sup>4,7</sup> The projector augmented wave (PAW)<sup>8</sup> method was used to describe the nuclei and core electrons interactions. The electron exchange correlation energy was calculated within the generalized gradient approximation (GGA) in the Perdew-Burke-Ernzerhof formalism (PBE).<sup>9</sup> DFT-D2 method<sup>10</sup> is applied to account for van der Waals interactions. The energy cutoff for the plane-wave basis expansion was set to be 400 eV. Periodic boundary conditions were used for all simulations. The simulation cell dimension was about 21.36 Å × 21.36 Å × 10.57 Å. The energy and force convergence criteria were set to be 10<sup>-4</sup> eV and 0.01eV/Å, respectively. The geometry of structure was optimized with conjugate gradient algorithm using the convergence criteria mentioned above. The optimized geometry was used to perform ab initio molecular dynamics (AIMD) simulations within the canonical ensemble (NVT) at different temperatures (87 K, 143 K, 213 K, 273 K, and 343 K). The temperature was controlled with the Nosé-Hoover thermostat.<sup>11,12</sup> For each temperature mentioned above, a 2.0 ps AIMD simulation with a time step of 1.0 fs was run and the initial 0.5 ps part was discarded for equilibration. Note: during AIMD simulations, the methoxy groups of optimized geometry were set to be flexible, whilst the rest of the

atoms were kept frozen.

### Breakthrough Experiment.

The samples were filled with the column and heated at 423 K for 12h for activation before breakthrough test. The carried gas ( $\text{He} \geq 99.99$ ) was through the adsorption bed for 1 h with a flow rate of  $5 \text{ ml min}^{-1}$ . Then, a gas mixture of  $\text{C}_3\text{H}_6/\text{C}_3\text{H}_8$  (50:50, V: V) was feed into the adsorption column. The gas mixture flow rate was  $5 \text{ ml min}^{-1}$ , which controlled by a mass flow controller. In this work, breakthrough experiment was carried out at 298 K, 100 KPa. The composition of effluent from adsorption bed is monitored by a gas chromatography.

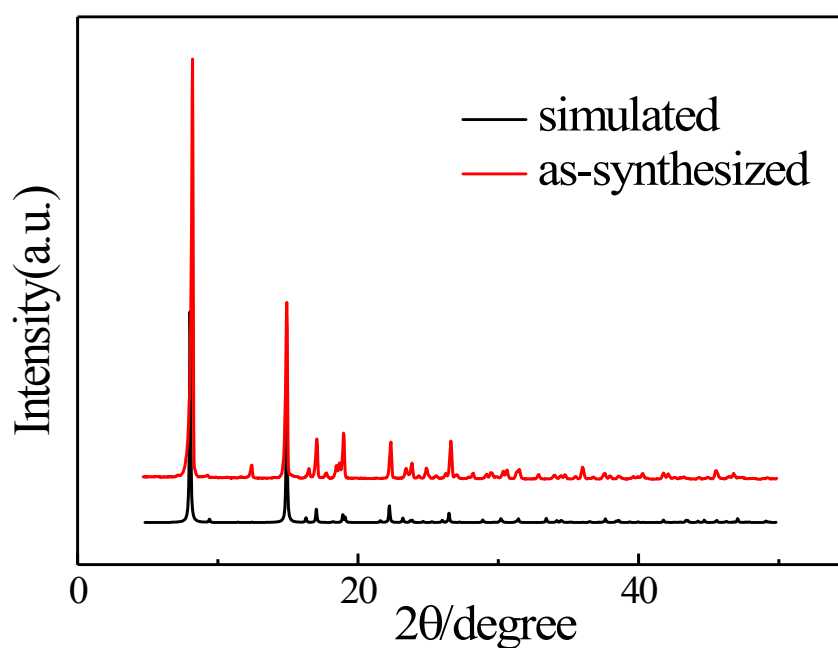


Fig. S1 PXRD patterns of CAU-10-OMe.

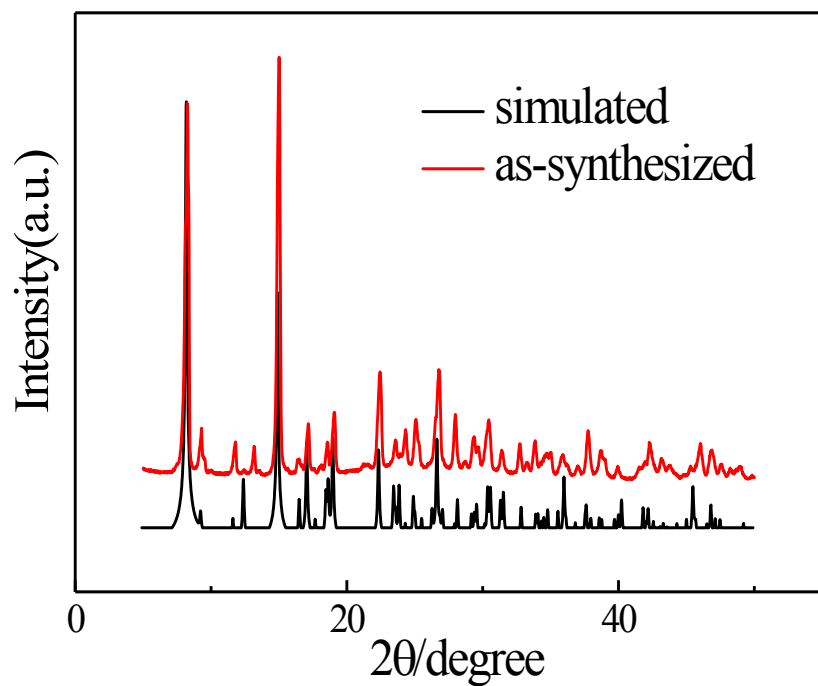


Fig. S2 PXRD patterns of CAU-10-H.

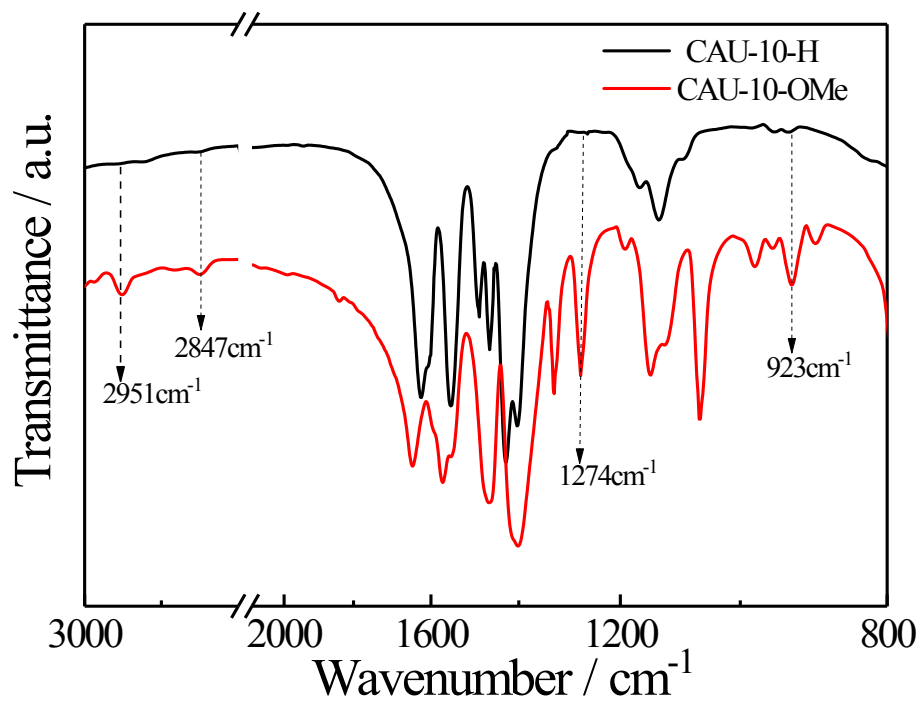


Fig. S3 FTIR spectra of CAU-10-H and CAU-10-OMe.

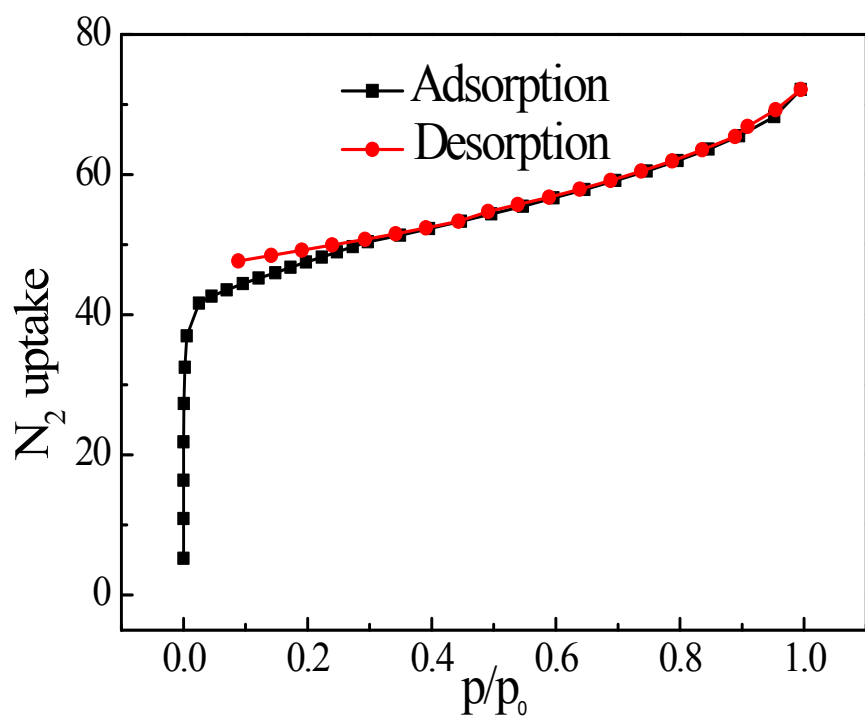


Fig. S4  $N_2$  adsorption-desorption isotherms at 77 K of CAU-10-OMe.

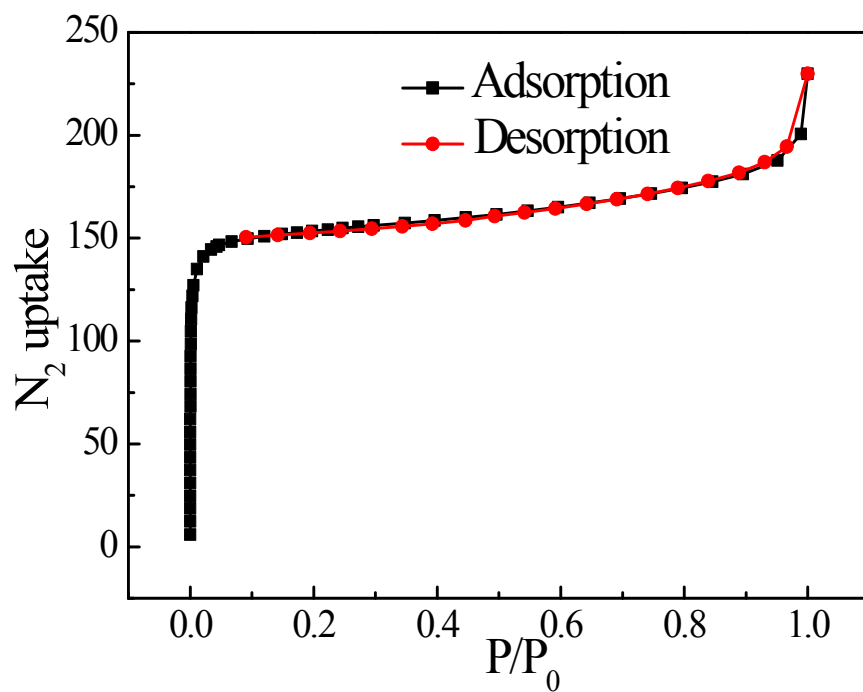


Fig. S5  $N_2$  adsorption-desorption isotherms at 77 K of CAU-10-H.



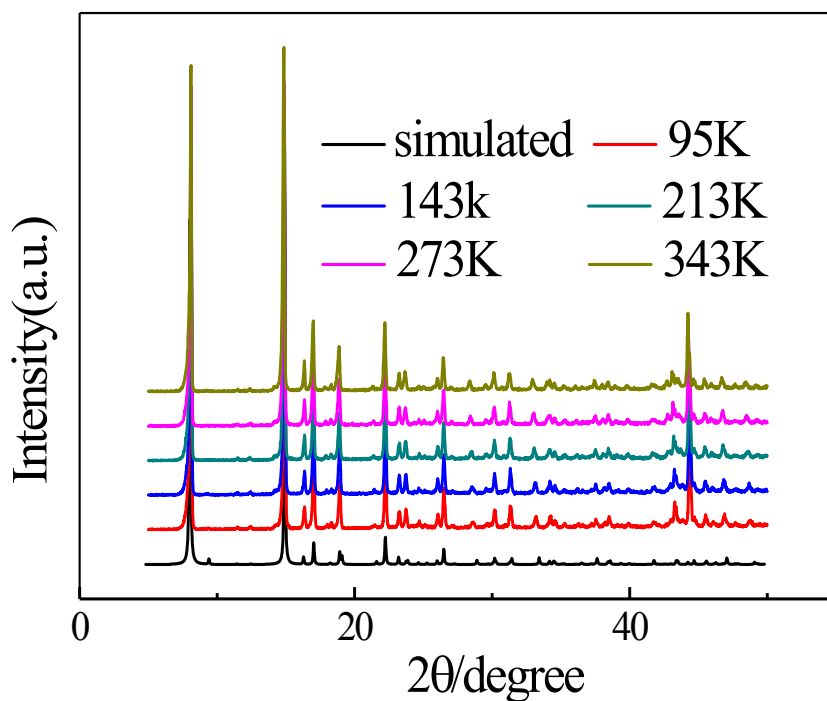


Fig. S6 Variable-temperature PXRD (VT-PXRD) patterns of CAU-10-OMe under air atmosphere.

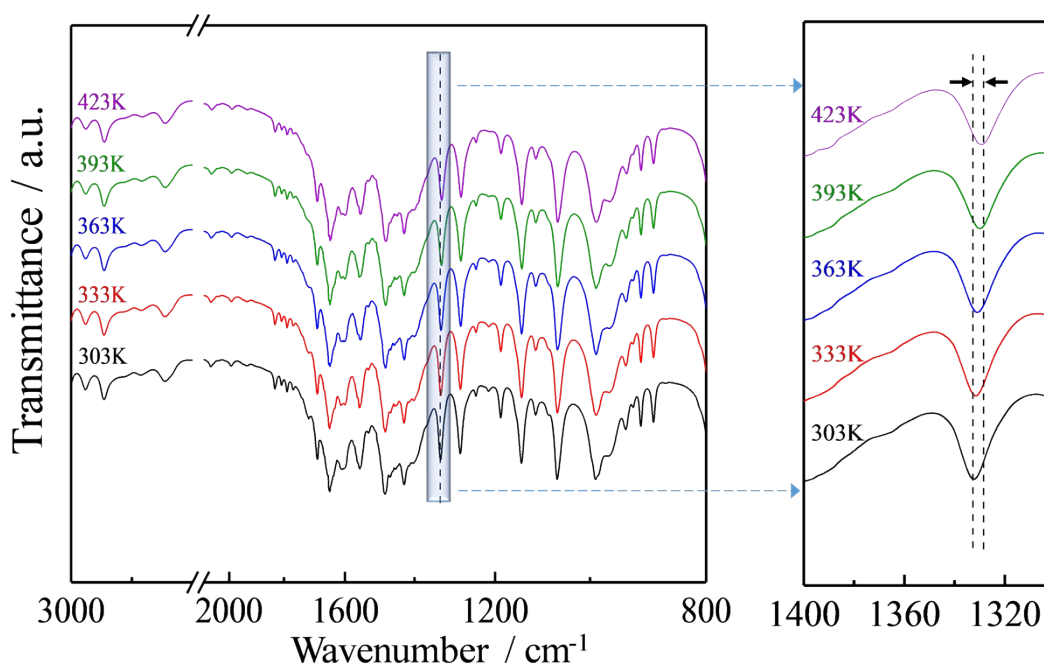


Fig. S7 Temperature dependence FTIR spectra of CAU-10-OMe.

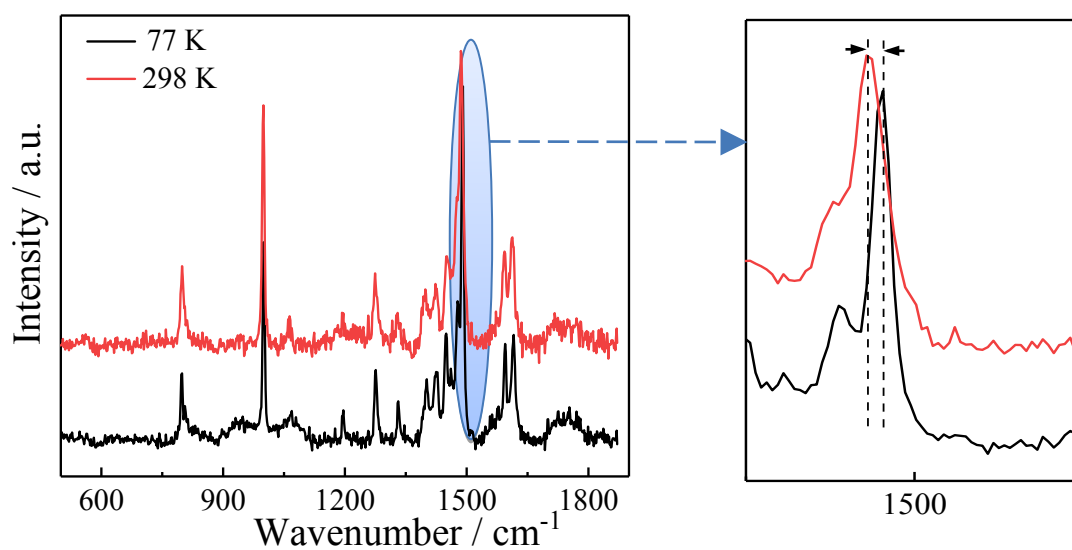


Fig. S8 Temperature dependence Raman spectra of CAU-10-OMe.

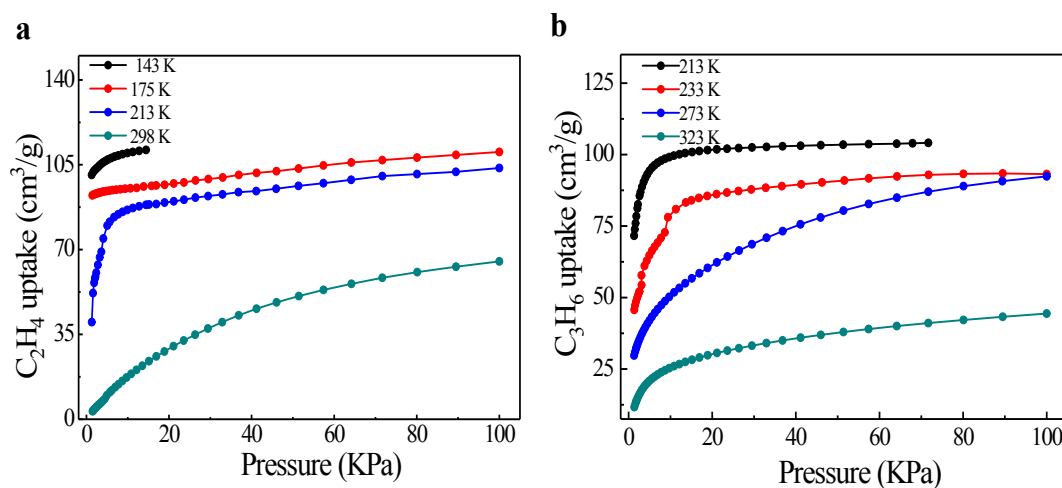


Fig. S9 The adsorption isotherms of  $C_2H_4$  (a) and  $C_3H_6$  (b) on CAU-10-H at 143 K - 323 K.

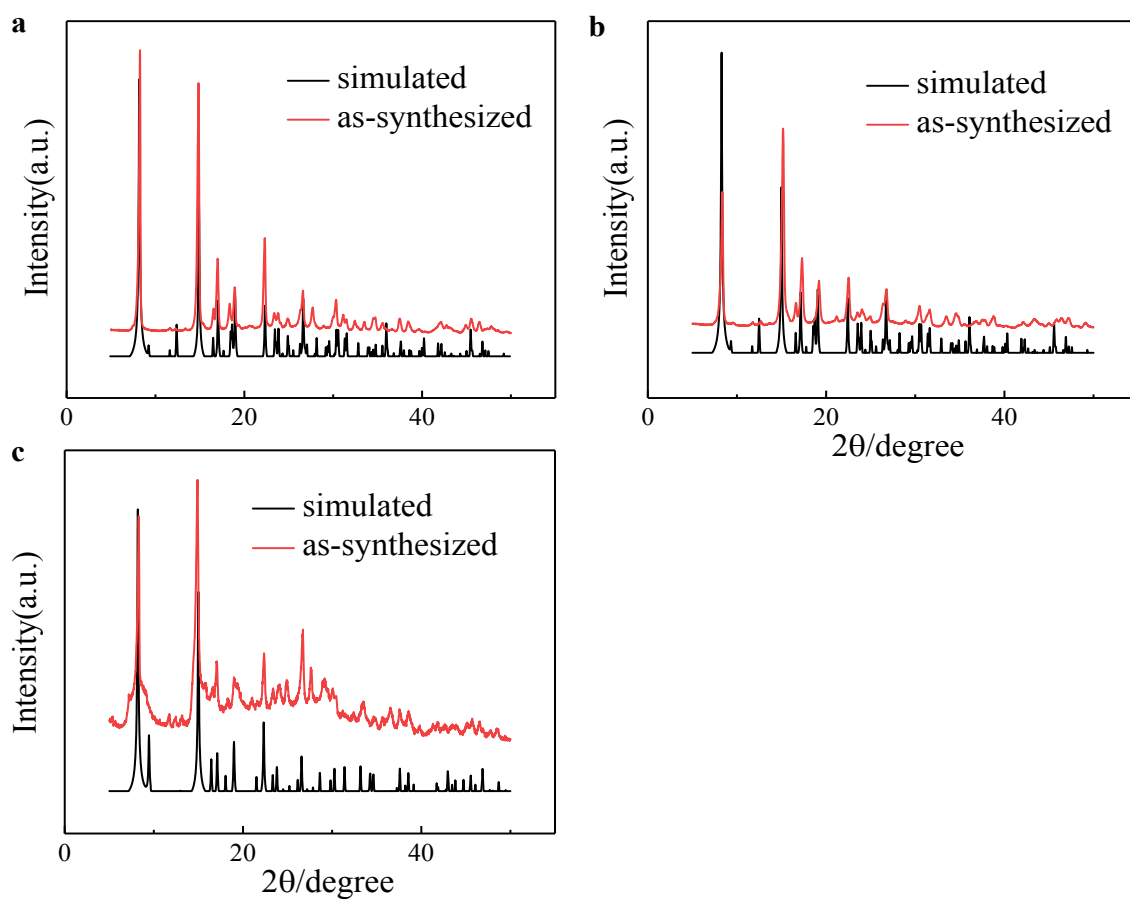


Fig. S10 PXRD patterns of CAU-10-NH<sub>2</sub> (a), CAU-10-NO<sub>2</sub> (b) and CAU-10-F (c).

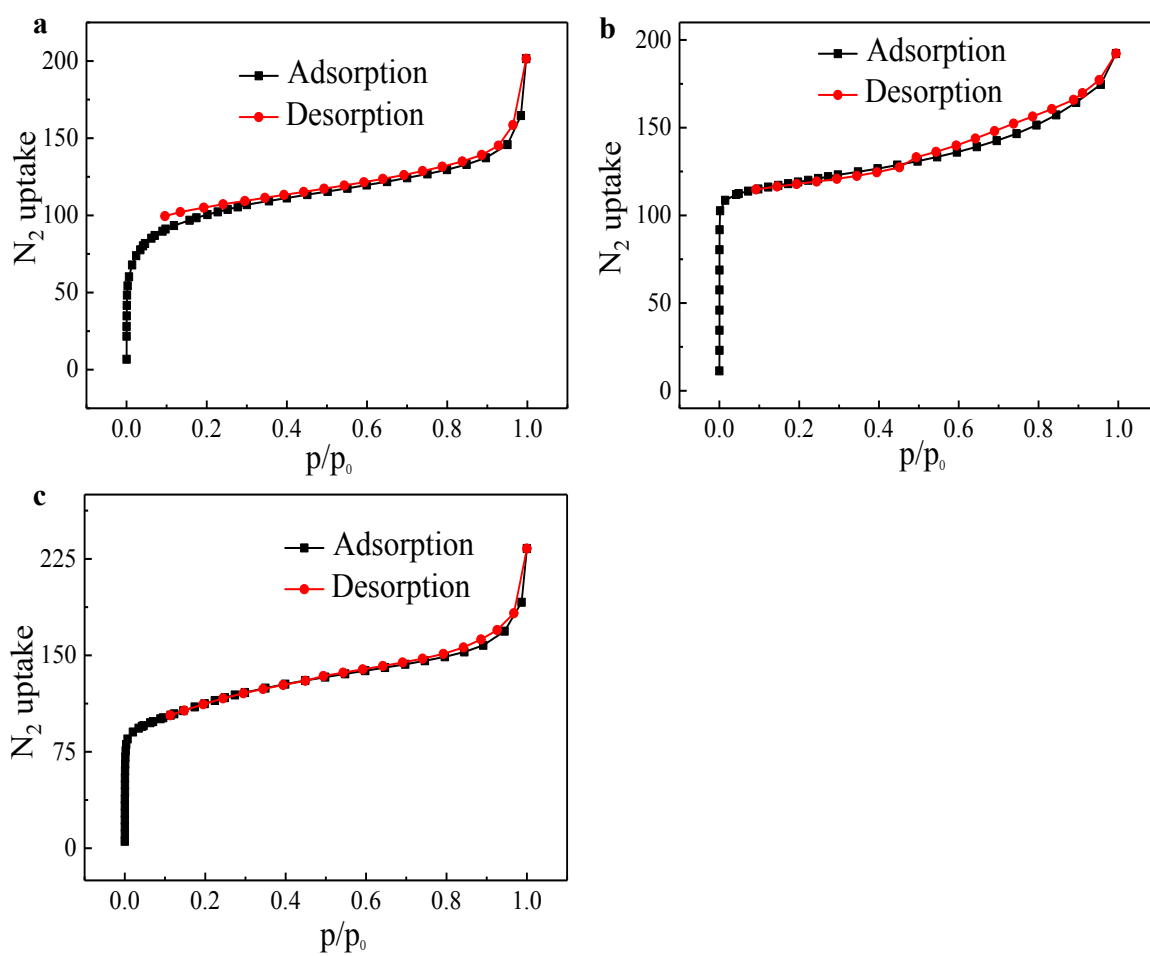


Fig. S11  $N_2$  adsorption-desorption isotherms at 77K of CAU-10-NH<sub>2</sub> (a), CAU-10-NO<sub>2</sub> (b) and CAU-10-F (c).

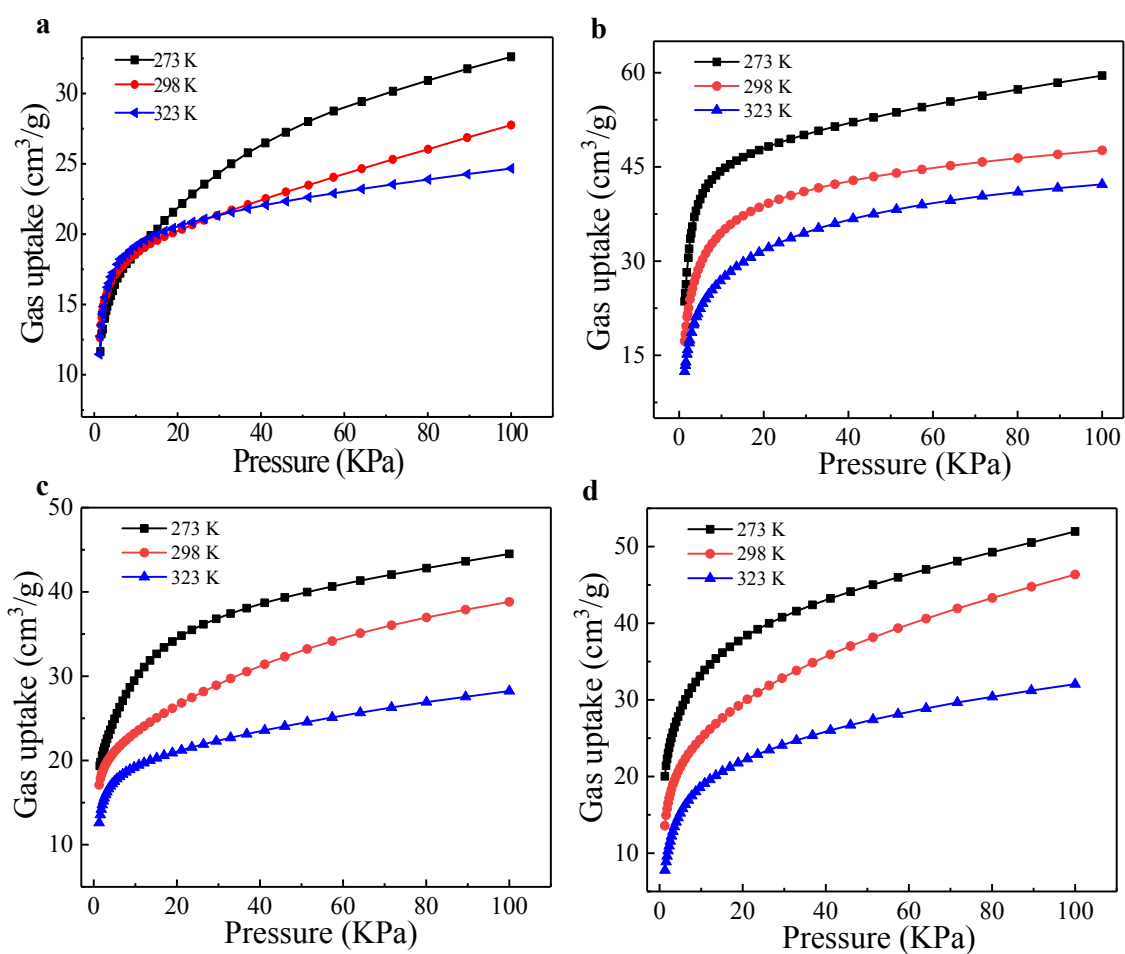


Fig. S12 The adsorption isotherms of  $C_3H_6$  on CAU-10-OMe (a), CAU-10-NH<sub>2</sub> (b), CAU-10-NO<sub>2</sub> (c) and CAU-10-F (d) at 273 K-323 K.

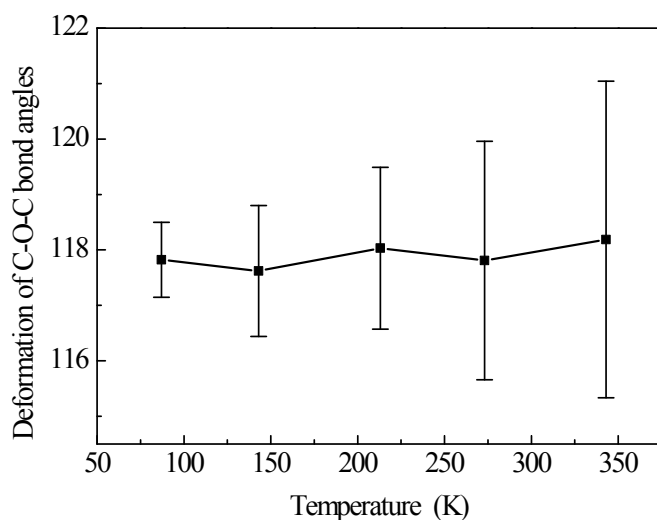


Fig. S13 AIMD simulated evolution of the C-O-C bond angles in the flexible methoxyl groups of CAU-10-OMe as a function of the temperature.

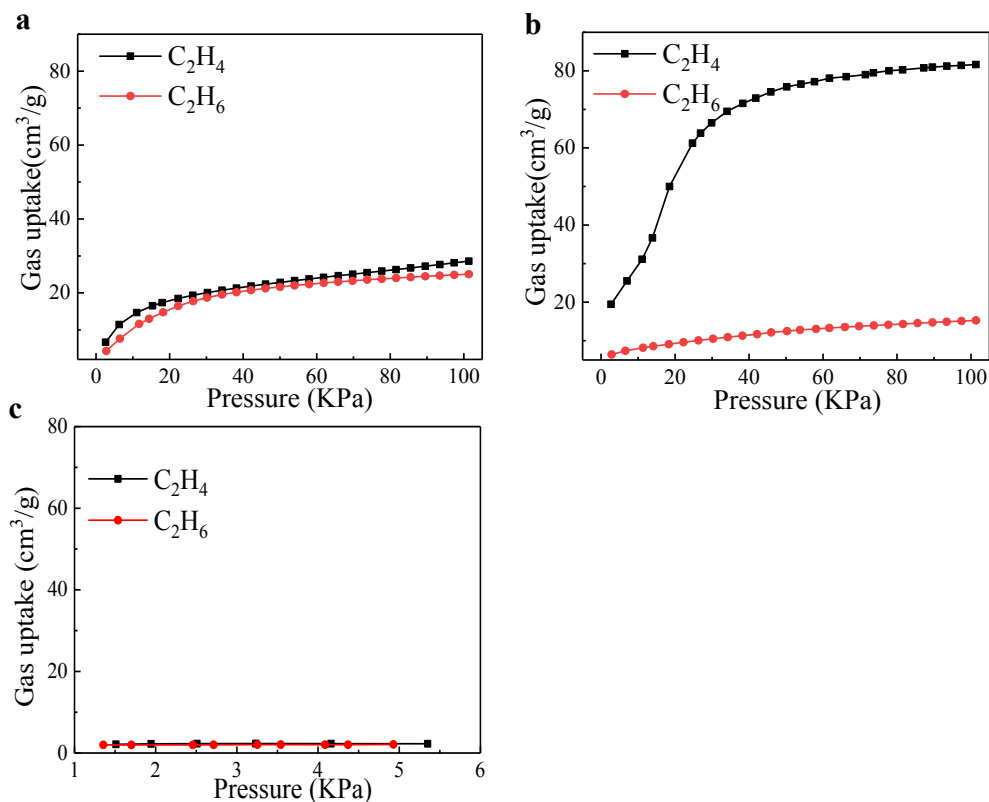


Fig. S14 The adsorption isotherms of  $C_2H_4$  and  $C_2H_6$  on CAU-10-OMe at 298 K (a), 203 K (b) and 143 K (c).

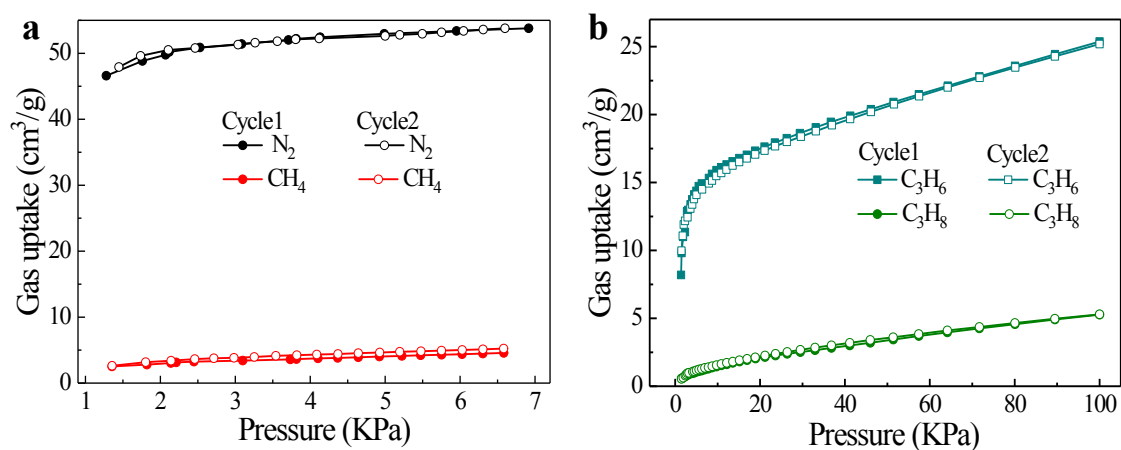


Fig. S15 Reversible adsorption of  $N_2/CH_4$  at 87 K (a) and  $C_3H_6/C_3H_8$  at 298 K (b) on CAU-10-OMe.

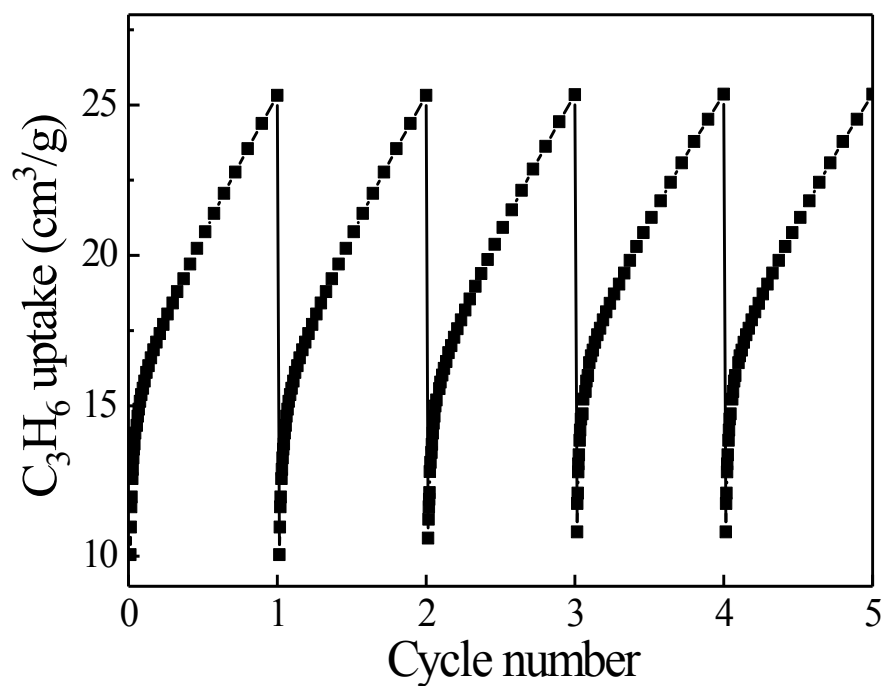


Fig. S16 Five cycles of  $C_3H_6$  adsorption-desorption on the CAU-10-OMe at 298 K and 100 KPa for adsorption and under dynamic vacuum at 423 K for 12 hours for desorption.

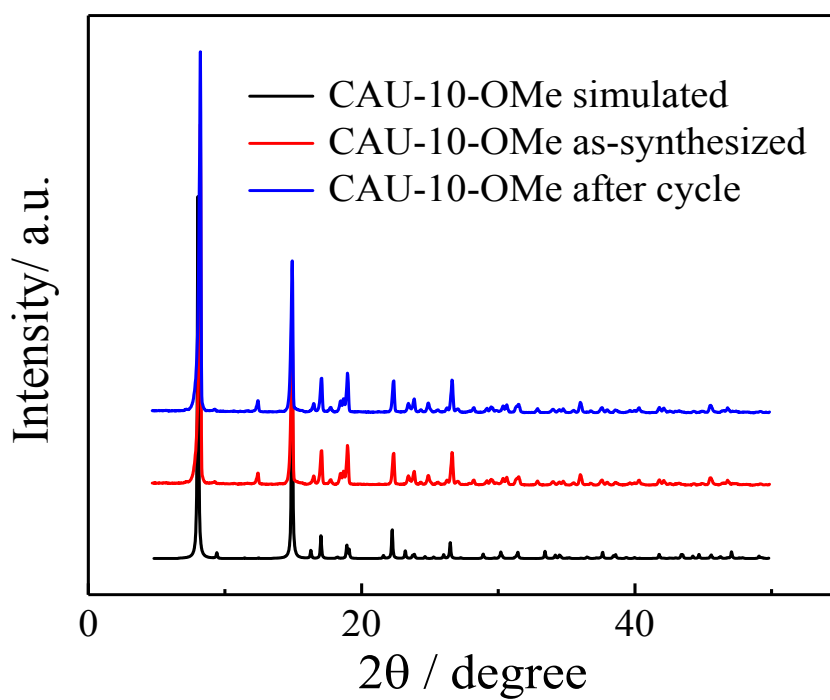


Fig. S17 PXRD result of CAU-10-OMe after cycle experimental.

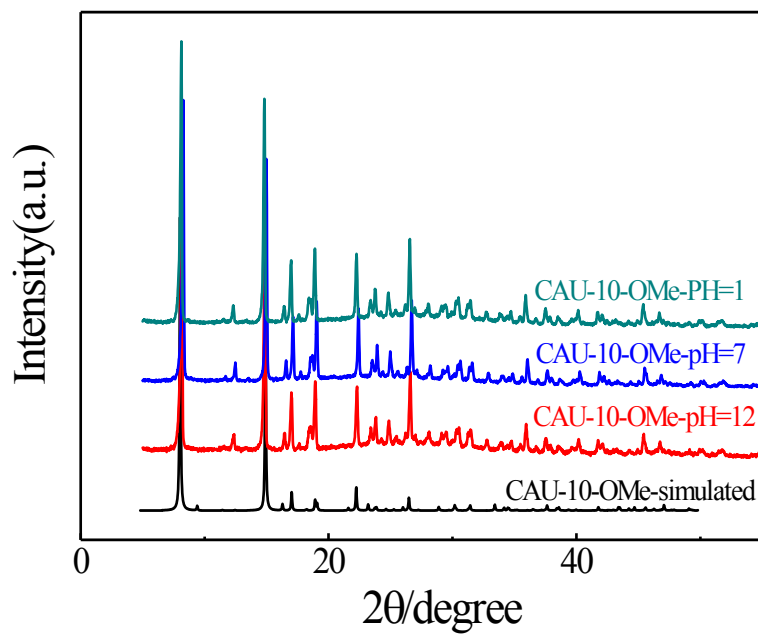


Fig. S18 Comparison of PXRD patterns of CAU-10-OMe after immersing water solution for 24h with different pH.



## Reference

- 1 H. Reinsch, M. A. van der Veen, B. Gil, B. Marszalek, T. Verbiest, D. de Vos, N. Stock, *Chem. Mater.*, 2012, **25**, 17-26.
- 2 R. E. Rondeau, *J. Chem. Eng. Data.*, 1966, **11**, 124.
- 3 A. M. Phipps, D. N. Hume, *J. Chem. Educ.*, 1968, **45**, 664.
- 4 G. Kresse, J. Hafner, *Phys. Rev. B*, 1993, **47**, 558-561.
- 5 G. Kresse, J. Furthmüller, *Comput. Mater. Sci.*, 1996, **6**, 15-50.
- 6 G. Kresse, J. Furthmüller, *Phys. Rev. B*, 1996, **54**, 11169-11186.
- 7 G. Kresse, J. Hafner, *Phys. Rev. B*, 1994, **49**, 14251-14269.
- 8 P. E. Blöchl, *Phys. Rev. B*, 1994, **50**, 17953-17979.
- 9 J. P. Perdew, K. Burke, M. Ernzerhof, *Phys. Rev. Lett.*, 1996, **77**, 3865-3868.
- 10 S. Grimme, *J. Comput. Chem.*, 2006, **27**, 1787-1799.
- 11 S. Nosé, *J. Chem. Phys.*, 1984, **81**, 511-519.
- 12 S. Nosé, *Mol. Phys.*, 1984, **52**, 255-268.